

3D-printed chemiluminescence flow cells with customized cross-section geometry for enhanced analytical performance

--Manuscript Draft--

| | |
|------------------------------|--|
| Manuscript Number: | |
| Article Type: | Research Paper |
| Section/Category: | Separation for Environmental and food applications |
| Keywords: | 3D-printing; flow-cell; chemiluminescence; flow injection; prototyping |
| Corresponding Author: | Manuel Miro, PhD University of Balearic Islands Palma de Mallorca, SPAIN |
| First Author: | Manuel Miro, PhD |
| Order of Authors: | Manuel Miro, PhD Lucia Garcia-Moll Alexandra Sixto, Dr. Enrique Javier Carrasco-Correa |
| Abstract: | <p>Low force stereolithography is exploited for the first time for one-step facile fabrication of chemiluminescence (CL) flow-through cells that bear unrivalled features as compared to those available through milling or blowing procedures or alternative 3D printing technologies. A variety of bespoke cross-section geometries with polyhedral features (namely, trigonal, cubic, and five-side prism) as well as semicircular cross-section are herein critically evaluated in terms of analytical performance against the standard cylindrical cross-section in a flat spirally-shape format. The idea behind is to maximize capture of elicited light by the new designs while leveraging 3D printing further for fabrication of (i) customized gaskets that enable reliable attaching of the active mixing zone of the CL cell to the detection window, (ii) in-line 3D printed serpentine reactors, and (iii) flow confluences with tailorable shapes for enhancing mixing of samples with CL reagents. Up to twenty transparent functional cells were simultaneously fabricated without inner supports following post-curing and surface treatment protocols lasting less than 5 h. In fact, previous attempts to print spirally-shaped cells in one-step by resorting to less cost effective photopolymer inkjet printing technologies were unsuccessful because of the requirement of lengthy procedures (> 15 days) for quantitative removal of the support material. By exploiting the phthalazinedione-hydrogen peroxide chemistry as a model reaction, the five-side irregular pentagon cell exhibited superior analytical figures of merit in terms of LOD, dynamic range and intermediate precision as compared to alternative designs. Computational fluid dynamic simulations for mapping velocities at the entry region of the spiral cell corroborated the fact that the 5-side prism flow-cell with Y-type confluence permitted the most efficient mixing of reagents and sample while enabling larger flow velocities near the inlet that contribute to a more efficient capture of the photons from the flash-type reaction. The applicability of the 3D printed 5-side prism CL cell for automatic determination of hydrogen peroxide using a computerized hybrid flow system was demonstrated for the analysis of high matrix samples, viz., seawater and saliva, with relative recoveries ranging from 83 to 103%.</p> |
| Suggested Reviewers: | <p>Wolfgang Frenzel, Dr. TU Berlin University wolfgang.frenzel@tu-berlin.de</p> <p>Spas Kolev, Prof. The University of Melbourne s.kolev@unimelb.edu.au</p> <p>Anthony Calokerinos, Prof. National and Kapodistrian University of Athens calokerinos@chem.uoa.gr</p> |

| | |
|---------------------------|--|
| | Ana Garcia-Campana, Prof. University of Granada amgarcia@ugr.es |
| | Xiangbao Long, Dr. Shanghai Jiao Tong University xblong2000@yahoo.com |
| | Marcin Wieczorek, Dr. Jagiellonian University in Krakow marcin.wieczorek@uj.edu.pl |
| Opposed Reviewers: | |

DEPARTMENT OF CHEMISTRY
University of the Balearic Islands
Carretera de Valldemossa km 7.5
E-07122 Palma de Mallorca, Illes Balears, Spain
Manuel Miró, PhD
Full Professor
E-mail: manuel.miro@uib.es
Tel: +34-971172746



Universitat
de les Illes Balears

Reviews Editor
Analytica Chimica Acta

Associate Editor
Encyclopaedia of Analytical Science, 3rd Ed.
Elsevier Ltd

November 1, 2022

Dear Jean-Michel and José Luis,

I am pleased to submit our original research article entitled “*3D-printed chemiluminescence flow cells with customized cross-section geometry for enhanced analytical performance*” for potential publication in Talanta as a full paper.

The attached files contain the full text of the manuscript, including references, tables, figures and figure legends.

The submitted manuscript is unpublished and has not been submitted for publication elsewhere.

Best regards from Mallorca,

Novelty Statement

This paper reports for the first time the design, optimization and fast fabrication of 3D printed stereolithographic chemiluminescence flow cells with entirely new cross-section geometries that are not available by standard milling or soft lithographic process nor by alternative inkjet photopolymer 3D printing protocols. The new designs afforded enhanced mixing of sample and reagents with large volume of reactants in close vicinity to the photomultiplier thus enabling maximum capture of elicited light from flash chemiluminescence reactions

Potential reviewers

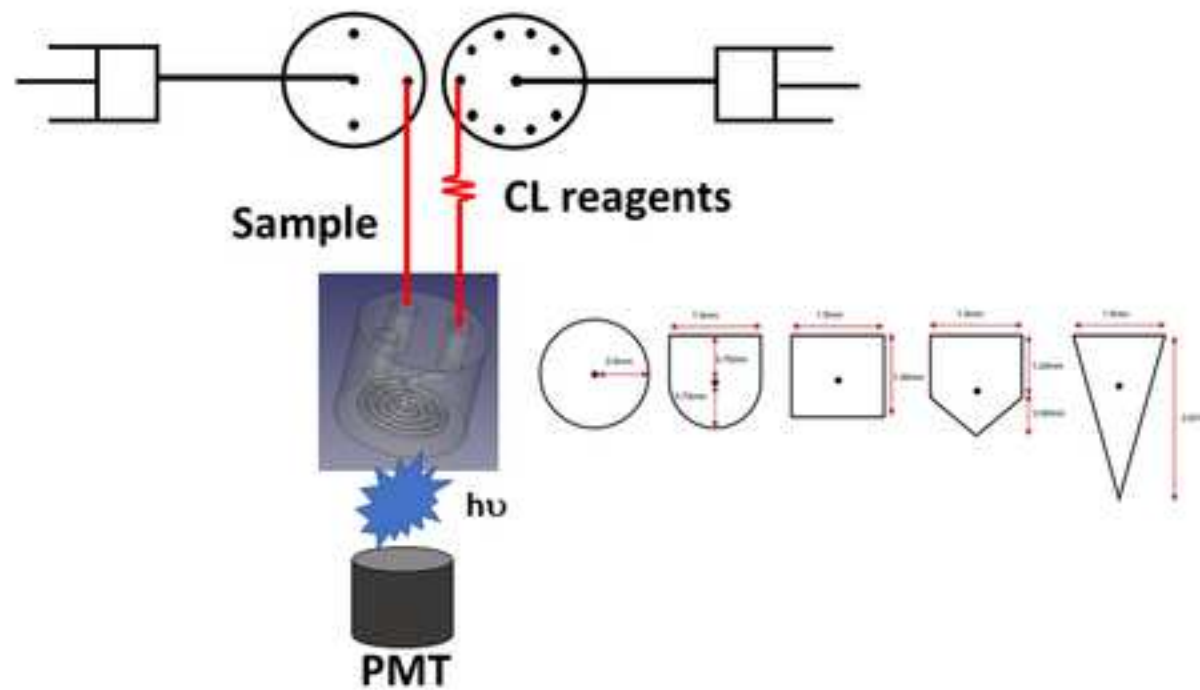
1. Dr. Wolfgang Frenzel, Technical University of Berlin, Germany.
E-mail: wolfgang.frenzel@tu-berlin.de
2. Prof. Spas Kolev, The University of Melbourne, Australia
E-mail: s.kolev@unimelb.edu.au
3. Prof. Anthony Calokerinos, University of Athens, Greece
E-mail: calokerinos@chem.uoa.gr
4. Prof. Ana Maria Garcia-Campaña, University of Granada, Spain
E-mail: amgarcia@ugr.es
5. Dr. Xiangbao Long, Shanghai Jiaotong University, China.
E-mail: xblong2000@yahoo.com; xblong2000@qq.com
6. Dr. Marcin Wiczorek, Jagiellonian University, Poland.
E-mail: marcin.wiczorek@uj.edu.pl

Low force stereolithography for facile prototyping of chemiluminescence flow cells

Unique cross-section geometries by 3D printing that are unavailable by milling

Postprocessing times of just a few hours compared to >15 days with photopolymer inkjet printing

Superior performance of the pentagonal geometry for luminol chemistry



3D-printed chemiluminescence flow cells with customized cross-section geometry for enhanced analytical performance

Llucia García-Moll^{a,1}, Alexandra Sixto^{b,1}, Enrique Javier Carrasco-Correa^{c*} and Manuel Miró^{a*}

a) FI-TRACE group, Department of Chemistry, University of the Balearic Islands, Carretera de Valldemossa km 7.5, E-07122 Palma de Mallorca, Spain

b) Cátedra de Química Analítica, Departamento Estrella Campos, Facultad de Química, Universidad de la República, Av. Gral. Flores 2124, 11800 Montevideo, Uruguay

c) CLECEM group, Department of Analytical Chemistry, University of Valencia, C/ Doctor Moliner, 50, E-46100 Burjassot, Valencia, Spain

Abstract

Low force stereolithography is exploited for the first time for one-step facile fabrication of chemiluminescence (CL) flow-through cells that bear unrivalled features as compared to those available through milling or blowing procedures or alternative 3D printing technologies. A variety of bespoke cross-section geometries with polyhedral features (namely, trigonal, cubic, and five-side prism) as well as semicircular cross-section are herein critically evaluated in terms of analytical performance against the standard cylindrical cross-section in a flat spirally-shape format. The idea behind is to maximize capture of elicited light by the new designs while leveraging 3D printing further for fabrication of (i) customized gaskets that enable reliable attaching of the active mixing zone of the CL cell to the detection window, (ii) in-line 3D printed serpentine reactors, and (iii) flow confluences with tailorable shapes for enhancing mixing of samples with CL reagents. Up to twenty transparent functional cells were simultaneously fabricated without inner supports following post-curing and surface treatment protocols lasting less than 5 h. In fact, previous attempts to print spirally-shaped cells in one-step by resorting to less cost effective photopolymer inkjet printing technologies were unsuccessful because of the requirement of lengthy procedures (> 15 days) for quantitative removal of the support material. By exploiting the phthalazinedione-hydrogen peroxide chemistry as a model reaction, the five-side irregular pentagon cell exhibited superior analytical figures of merit in terms of LOD, dynamic range and intermediate precision as compared to alternative designs. Computational fluid dynamic simulations for mapping velocities at the entry region of the spiral cell corroborated the fact that the 5-side prism flow-cell with Y-type confluence permitted the most efficient mixing

¹ Both authors have equally contributed to this work.

* Corresponding authors. E-mails: enrique.carrasco@uv.es (E.J. Carrasco-Correa), manuel.miro@uib.es (M. Miró)

36 of reagents and sample while enabling larger flow velocities near the inlet that contribute to a
37 more efficient capture of the photons from the flash-type reaction. The applicability of the 3D
38 printed 5-side prism CL cell for automatic determination of hydrogen peroxide using a
39 computerized hybrid flow system was demonstrated for the analysis of high matrix samples, viz.,
40 seawater and saliva, with relative recoveries ranging from 83 to 103%.

41

42 **Keyword:** 3D-printing, flow-cell, chemiluminescence, flow injection, prototyping

43

44 INTRODUCTION

45 Additive manufacturing, commonly termed 3D printing, can be categorized as an interdisciplinary
46 technique in a wide range of fields of research, including (bio)analytical science [1-3]. In this
47 context, 3D printing has opened new avenues in the design and fast prototyping by iterative
48 changes using computer-aided modelling of optical and electrochemical (bio)sensing platforms
49 [2,4,5], integrated and functional microscale/flow-injection devices [6-8], porous materials for
50 sample preparation/microextraction [7-11], and chromatographic separation phases [1,12] with
51 dedicated functionalities. Possibilities for tailor-made fabrication of devices with intricate
52 features using photopolymerizable or thermoplastic materials are, in principle, merely limited by
53 our own imagination, yet most of the research to date has been geared towards printing of simple
54 scaffolds, holders, templates or housing that are introduced in any of the steps of the analytical
55 process including the analytical measurement/detection step [2,13]. Out of the assortment of 3D
56 printing technologies launched to the market, fused deposition modelling (FDM) using affordable
57 consumer-grade printers has attracted a great deal of attention for production of one-step bespoke
58 prints that are adaptable to analytical detection systems [14]. Interesting examples are found in
59 recent literature reporting the fabrication of customizable and versatile electrochemical cells and
60 electrodes using conductive filaments [15] along with scaffolds and detection cells with
61 adjustable optical length [16], and customized arrangements for optical detection to which light
62 emitting diodes, photodiodes and/or optical fibers are readily integrated [17]. An additional
63 advantage of multimaterial FDM printers is the possibility of simultaneous usage of filament
64 materials with distinct optical transparency features that demonstrated utility for minimization of
65 stray light in photometric cells [18]. However, the limited chemical compatibility of commonly
66 used thermoplastics (e.g., polylactic acid) [16], and the inability to withstand moderate flow
67 pressures [17] make the actual applicability of FDM for printing of flow-through detection
68 platforms debatable. The improved chemical and flow resistance (water tight prints) of alternative
69 additive manufacturing technologies (*viz.*, vat polymerization (also called stereolithography, SL)
70 or photopolymer inkjet printing (PIP)) that enable (i) higher throughput for fabrication of multiple
71 devices, (ii) minimal feature sizes (layer thickness) and (iii) improved quality surface finishes
72 against FDM can be fully leveraged for expanding the applicability of 3D printing to fabricate

1 73 detection components in flow injection setups [**Error! Bookmark not defined.**]. In both
2 74 techniques, a light source selectively cures a photopolymer liquid resin on a moving platform by
3 75 using (i) UV-curing lamp (PIP), (ii) laser beam (low force stereolithography, LFS) or (iii) LED
4 76 in the absence of masks (digital light processing, DLP) [19]. Notwithstanding the advantageous
5 77 features of LFS/DLP and PIP for potential fabrication of functional devices with entirely new
6 78 formats, little effort has been dedicated to build flow-cells and functional components of
7 79 luminescence detection systems, in particular, for chemiluminescence (CL) detection. Standard
8 80 quartz flow cells are of rigid architecture, with pre-defined inner volume and dimensions so that
9 81 redesign by glass blowing needs specialist infrastructure [20,21]. Polymeric tubing for assembling
10 82 flat flow-cells is also limited by available ID dimensions, and the reproducible mounting of the
11 83 coiled tubing onto the photodetector might be a daunting task [22]. To shed light on the
12 84 opportunities of 3D printing in the CL detection field, the seminal work by Francis' group [23] in
13 85 which bespoke 3D printed PIP flow-cells were critically compared against CNC milled
14 86 counterparts for ameliorating mixing efficiency and light capture from permanganate chemistry-
15 87 based reactions is worth mentioning. Unfortunately, the authors did not succeed in fabricating
16 88 closed channels for the CL printed cells because of technical issues for quantitative
17 89 removal/melting of the support wax inside the channels even after heating at 70°C and sonication
18 90 at high temperature. Hence, they opted for a multi-stage fabrication process of open spiral
19 91 channel, thus resembling the steps of milling schemes, with further sealing by application of a
20 92 transparent epoxy-acetate film operating as a window. Mounting of the printed CL onto the
21 93 photodetector was also not straightforward and a purpose-build aluminium holder incorporating
22 94 a reflective element was needed for comparable performance with that of milled cells [23].
23 95 Further studies by Gupta *et al.* [24] in which the wax was replaced by a water-soluble support
24 96 material revealed that post-PIP processing of closed spiral cells with soaking in alkaline solution
25 97 and intermittent sonication required more than 15 days for complete clearance of the support.
26 98 This lengthy rinsing procedure corroborated the unsuitability of PIP printing for 3D fabrication
27 99 of analytical flow-cells with tortuous structure. In addition, the high start-up expenses of PIP
28 100 printing negate its actual applicability for affordable and fast prototyping of analytical devices.

29 101 In this work, we demonstrated for the first time the unique opportunities of LFS for one-step
30 102 simple fabrication of flow-through CL cells bearing tortuous spirally-shaped geometry with rapid
31 103 post-LFS processing in a few hours. To simplify the assembly of the detection components, a
32 104 rugged press-fit mounting of the bespoke 3D printed cell onto the active area of the photodetector
33 105 is ensured by a printed ring-shaped housing. More sophisticated 3D channel designs
34 106 encompassing unrivalled cross-section geometries that are inaccessible by CNC milling processes
35 107 and diverge from the traditional circular sections of standard flow-cells are also to be herein
36 108 evaluated in terms of analytical performance using the phthalazinedione chemistry for

109 determination of reactive oxygen species as a proof of concept applicability. The idea behind is
110 to assess the effect of several polyhedral shapes (namely, trigonal, square, and five-side prism) as
111 well as semicircular shapes of CL cells and fluidic confluences for efficient mixing and capture
112 of elicited light in the vicinity of the detection system. To this end, a simple and fully automatic
113 two-syringe flow arrangement was assembled for rapid mixing of reactants and analyte aiming at
114 detection of hydrogen peroxide in biological and marine samples at concentration levels
115 significantly lower than those reported using alternative radial-shaped printed flow cells [24].

116

117 **EXPERIMENTAL**

118 **Reagents and solutions**

119 All the chemicals, unless otherwise stated, were of analytical reagent grade. Solutions were
120 prepared using Milli-Q water (Merck-Millipore, Darmstadt Germany) with a resistivity ≥ 18.2
121 $\text{M}\Omega\cdot\text{cm}$. The chemiluminogenic reagent consisted of 0.5 mmol/L 3-aminophthalhydrazide
122 (luminol) (Sigma-Aldrich/Merck KGaA, Darmstadt, Germany) dissolved in 1 mol/L NH_4OH
123 (Fisher Scientific SL, Madrid, Spain) and 0.1 mol/L K_2CO_3 (Fisher Scientific). The reagent was
124 let stand for at least three days at 4°C in the dark pending use followed by pH adjustment to 10.8
125 with concentrated HCl (Fisher Scientific). A 0.25 mmol/L Co(II), used as a catalyser, was
126 prepared from $\text{Co}(\text{NO}_3)_2\cdot 6\text{H}_2\text{O}$ (Fisher Scientific).

127 An intermediate standard solution of 0.1 mol/L H_2O_2 (Sigma-Aldrich/Merck KGaA) was titrated
128 against 0.2 mol/L KMnO_4 (Fisher Scientific) twice a week and working standard solutions were
129 prepared just before analysis. The permanganate reagent was titrated weekly against sodium
130 oxalate (Fisher Scientific). Working standard solutions of H_2O_2 were prepared by serial dilution
131 of the stock within the concentration range spanning from 50 nmol/L to 1000 nmol/L.

132 Fluidic platforms (flow-through cells and mixing coil) were 3D printed by resorting to the
133 FLGPCL02 (Formlabs, Barcelona, Spain) clear resin. Isopropyl alcohol (IPA, Fisher Scientific)
134 was used for removal of the resin residues within the channels of the 3D printed devices.

135 Seawater surrogate was prepared according to Weztel and Likens' recommendations [25] by
136 dissolving the following salts and ingredients in Milli-Q water: 3.0 mg L^{-1} NaF, 20 mg L^{-1}
137 $\text{SrCl}_2\cdot 6\text{H}_2\text{O}$, 30 mg L^{-1} H_3BO_3 , 100 mg L^{-1} KBr, 700 mg L^{-1} KCl, 1470 mg L^{-1} $\text{CaCl}_2\cdot 2\text{H}_2\text{O}$,
138 4000 mg L^{-1} Na_2SO_4 , 10,780 mg L^{-1} $\text{MgCl}_2\cdot 6\text{H}_2\text{O}$, 23,500 mg L^{-1} NaCl, 20 mg L^{-1}
139 $\text{Na}_2\text{SiO}_3\cdot 9\text{H}_2\text{O}$, and 200 mg L^{-1} NaHCO_3 , all of them from Fisher Scientific SL. Human saliva
140 matrix (5 mL) was collected from a healthy volunteer aged > 18 yr by spitting in a polypropylene
141 tube just before analysis, filtrated through a 0.45 μm nylon filter, and diluted 1:400 previous
142 hydrogen peroxide determination. The participant provided informed consent before participating

143 in this project that was approved by the Research Ethics Committee of the Balearic Islands (ID
144 no. IB 3776/18 PI).

145 **Fabrication of the 3D printed devices**

147 The LFS fluidic devices (CL flow-through cell and mixing coil) were modelled via the freeware
148 FreeCAD software (www.freecadweb.org). Five flow-through spirally-shaped cells with different
149 cross-sectional channel geometry were designed and one-step printed (see Fig. S1): cylindrical,
150 semicylindrical, pyramidal shape, cubic and 5-side prism (irregular pentagon). The overall cells
151 were fabricated in cylindrical-shaped modules with an outer diameter of 25 mm and height of 21
152 mm. Notwithstanding the distinct geometrical features, all cells bear a nominal length of 110 mm
153 and a nominal total volume of 221 μL . The enclosed channel geometries were devised aimed at
154 maximizing the volume of reactant zones in close contact with the detector window for efficient
155 capture of light from the flash CL reaction. Thus, the polyhedral base of the semicylindrical,
156 pyramidal, cubic or 5-side prism channels, all 1.5 mm wide, was attached to the photomultiplier
157 (PMT) window (see Fig. S1). The standard cylindrical cell was fabricated with an 0.8 mm ID so
158 as to bear identical inner volume than that of the rest of designs, and served as a reference for
159 evaluating the performance of the novel channel configurations.

160 The spirally-shaped flat flow-cells ended on one side with an integrated T-shaped upright
161 connector of 1.5 mm ID to mix the reagents (luminol and Co(II)) with the sample at straight angle
162 (Fig. S2A). Two inlets of 5.5 mm ID and 8 mm length each were printed on top of the connector
163 for tapered thread coupling of the CL cell with the flow system using nuts and flangeless tubing
164 (Fig. 1A and 1B). Alternative Y-shaped and Y'-shaped connectors were also evaluated for the
165 sake of improving mixing (Fig S2B and S2C). Both configurations were modelled to have
166 protruding channels of 1.5 mm ID and identical inlets than those of the T-shaped counterpart. The
167 main difference relies on the angles connecting the inlets with the outlet conduit, namely 135°
168 angle tilt relative to the outlet (Fig. S2B and S2C). The other end of the spirally shaped cell
169 consists of an upright outlet of 5.5 mm ID for tapered thread connection to waste (see Fig. 1A).

170 The flexibility of 3D printing was leveraged for fabrication of 3D serpentine coils for proper
171 mixing of the reagents (luminol and Co(II)) prior to downstream merging the sample (Fig. 1C).
172 The overall size of the units was 15 mm long, 15 mm wide and 29 mm high. The coil was designed
173 to have a 50 mm effective length with a 2 mm ID conduit and turnings of 5.3 mm diameter that
174 were 3 mm distant each other. Further, a cylindrical ring (47 mm OD and 26 mm ID) was printed
175 for reliable mounting of the flow-cell face-to-face to the PMT by press-fitting.

176 The STL files of the bespoke 3D platforms were loaded in the manufacturer's software (Preform,
177 Formlabs) for slicing and orientation prior to 3D printing via the LFS Form 3 printer (Formlabs,

178 Somerville, MA, USA). The devices were printed at a nominal resolution of 50 μm (440 layers
179 as a trade-off between speed and resolution of the final print) using the FLGPCL02 (Formlabs)
180 clear resin. All devices were printed with the spirally shaped channel face downward using 3 mm-
181 high outer supports onto the confluence face to facilitate their removal from the build platform
182 without jeopardising the surface properties (e.g., smoothness, transparency) of the face to be
183 coupled to the PMT.

184 After retrieving the 3D printed devices from the printer, the “green” objects were post-processed
185 by a multi-step operational procedure. Briefly, the devices were soaked in isopropyl alcohol (IPA)
186 for 10 min in an ultrasonic bath to remove the non-polymerized resin. Then, the closed channels
187 were manually perfused with *ca.* 50 mL IPA to eliminate remnants of liquid resin. Afterwards,
188 the prints were soaked in water for 10 min in an ultrasonic bath, followed by a third ultrasonic-
189 based cleaning procedure, now in IPA. Finally, the 3D printed devices were dried with nitrogen
190 and UV-postcured for 1 h under a 16 W low pressure mercury lamp UV oven (KA-9180, PSKY,
191 China) to harden the polymerized resin and prevent unspecific leaching of non-polymerized
192 oligomers. Once the post-printing process was finished, the two inlets and outlet of the CL cells
193 were manually tapered to 1/4" - 28 threads. The 3D flow-cells were finally sanded consecutively
194 with 1000 and 3000 grain sandpaper on the spiral channel face in order to improve their
195 transparency for CL measurements and fit it tightly to the PMT. To make the flow-cell even more
196 transparent, a minute amount of clear resin was manually applied after sanding to the external
197 face, homogenized by rubbing and finally post-cured *ca.* 3 h under 16 W UV light.

198 To study the inner channel structure and the possible reactivity of the printed devices, several
199 optical characterization studies were carried out by scanning electron microscopy (HITACHI S-
200 3400N, Ibaraki, Japan) and attenuated total reflection-infrared spectroscopy (Bruker, Germany).

201

202 **Flow manifold and chemiluminescence detection**

203 A diagrammatic representation of the flow manifold for evaluation of the 3D-printed flow-cells
204 aimed at the CL detection of hydrogen peroxide is presented in Fig. 1. The system is composed
205 of two automatic bi-directional syringe pumps (SP, Cavro, Tecan, Sunnyvale, USA) equipped
206 with gas-tight glass syringes (Hamilton, Bonaduz, Switzerland). One pump, used for the samples
207 or standards (SP2), was fitted with a 1 mL glass syringe and a three-way valve (VICI AG
208 International, Schenkon, Switzerland) on its head, which allowed connection with the flow
209 manifold or the solutions to be analyzed. The other pump (SP1) furnished with a 5 mL glass
210 syringe and a 9-port selection valve (VICI AG International) on its top, was used for in-situ
211 mixing the two CL reagents (luminol and Co(II)) in-syringe. The reagent mixture was herein
212 employed as a carrier solution. All the connections were made from 0.8 mm i.d. fluorinated
213 ethylene-propylene (FEP) tubing. The 3D-printed serpentine mixing coil (see Fig. 1) was

214 connected between the 9-port selection valve of SP1 and the flow-through cell for further
215 improvement of the mixing of reagents.

216 A photomultiplier H9319 (Hamamatsu, Shizuoka, Japan) with an optical window of 22 mm was
217 selected as a photodetector. The 3D printed spirally-shaped flow-cell mounted over the detector
218 window and integrating a flow confluence (see Fig. 1) permitted reagents and sample to be mixed
219 directly in front of the photomultiplier tube (PMT). The overall CL detection components were
220 arranged in a light-tight home-made box.

221 Cocosoft 5.16 software package written in Python [26] is utilized in this work for fully automatic
222 metering of the sample/reagent volumes, and controlling of the position of the multi-position
223 valves, speed of the SP, and acquisition of CL data. The CL peak height integrated by
224 Chromophoreasy.xlsm [27] was used as the analytical signal throughout.

225 226 **Flow-based analytical procedure**

227 Prior to use for the first time, the flow-through cell was flushed with luminol/Co(II)/700 nM H₂O₂
228 and filled with CL reagent overnight for further leaching of non-polymerized oligomers and cross-
229 linking agents (urethane and acrylate moieties) under alkaline conditions while serving for cell
230 ageing/passivation to obtain low baseline CL levels and repeatable analyte readouts afterwards.

231 The automatic flow method starts by filling the reagent channels with 250 μL of luminol (from
232 port 4, see Fig. 1) and 200 μL of Co(II) (from port 1) through the 9-position head valve from SP1,
233 and 200 μL of sample or standard solution through the three-way valve from SP2, which are
234 whereupon directed to waste. Then, SP1 is rinsed with 500 μL of luminol at 2000 $\mu\text{L min}^{-1}$.
235 Afterwards, SP2 is set to aspirate 380 μL of sample/standard from which 80 μL were dispensed
236 towards the manifold to fill the communication line between SP2 and the flow-through cell.
237 Afterwards, SP1 is programmed to aspirate five segments of 960 μL of luminol at 5000 $\mu\text{L min}^{-1}$
238 that are interdispersed in-syringe in tandem with four 50 μL segments of Co(II) aspirated at
239 2000 $\mu\text{L min}^{-1}$. Then, 700 μL of the *in-situ* mixed Co(II)-luminol reagent is dispensed forward
240 through the 3D printed flow-through mixing reactor at 1000 $\mu\text{L min}^{-1}$ towards the 3D-printed
241 flow-cell for recording of the background CL signal. At this moment, data acquisition is
242 automatically initiated and is followed by performing six replicate injections of 50 μL of sample
243 or standard every 23 s at 1500 $\mu\text{L min}^{-1}$ into a continuously flowing reagent stream of luminol-
244 Co(II) composite reagent at 1000 $\mu\text{L min}^{-1}$. In the case of the T-confluence and because of
245 unwanted dispersion of the reagent flowing stream into the sample, while keeping it stagnant,
246 prior to inject the next sample plug, a burst of 10 μL of sample is pumped forward to rinse the
247 sample channel, and thus fresh sample is available to react with the CL reagent. To minimize
248 analyte carryover, SP1 was rinsed with 1 mL of Milli-Q water at 2500 $\mu\text{L min}^{-1}$ prior to analysing

249 the ensuing standard or sample. At the end of the working day, the manifold was cleaned with 5
250 mL of 0.5 mol L⁻¹ HCl followed by flushing with 10 mL of Milli-Q water at 5000 μL min⁻¹.

251 252 **Computational fluid dynamics**

253 The investigation of the fluid dynamics of the reagent and the sample zones at the confluence
254 point towards the inlet of the distinct spirally-shaped CL cells was performed using the freeware
255 Simscale (www.simscale.com). The simulations were undertaken at the time that the standard or
256 sample is injected along with the mixed reagent in the flow system at the flow-rates indicated
257 above using water as the solvent in all cases. The fluid dynamics were estimated based on the k-
258 omega SST model, the steady-state time dependency and the SIMPLE algorithm options using
259 incompressible analysis. Color mapping near the inlet of the spirally shaped cells that stands for
260 distinct ranges of flow rates was provided by Simscale.

261

262 **RESULTS AND DISCUSSION**

263 **Physicochemical characterization of the 3D printed flow-cells**

264 The actual channel cross-section features of the 3D printed spiral flow-cells as obtained LFS using
265 the consumer-grade Form 3 printer were evaluated by SEM. To this end, short open-ended
266 channels with the distinct five geometries (cylindrical, semicylindrical, pyramid shape, cubic and
267 5-side prism) were 3D printed and characterized. As shown in Fig. 2, the SEM images enable
268 elucidating the printing accuracy of the various CAD cross-section geometries for the spirally-
269 shaped channels.

270 Table 1 compiles the real volume of the different flow-cells, estimated from the actual features of
271 the SEM micrographs, and the printing precision of several prints (n = 3) of every flow-cell as
272 compared to the nominal volume (221 μL). As can be seen in Table 1, the volume difference %
273 is, in general, acceptable for practically all of the flow-cell geometries (<4.3%), except for the
274 pyramidal shape geometry with deviations as high as 25%. This observation is attributed to the
275 limited resolution of the LFS printer at the vertex of the triangle legs that causes resin
276 crosspolymerization with the consequent deviation from the triangular expected shape of the
277 structure. It should be noted that the low volume difference of the cubic shape is most likely a
278 consequence of the fact that point-by-point polymerization is more reliable for polyhedral features
279 with rectangular angles. Acceptable intermediate precision was found for all the geometries, yet

280 higher values were found for the pyramidal shape geometry (7.2% RSD) because of technical
281 issues for reliable fabrication of triangular shapes in non-supported 3D printed structures.

282 One of the potential problems related with 3D printing in milli/microfluidic platforms refers to
283 the surface chemical changes that the 3D printed photopolymer might undergo due to the
284 intermittent/continuous pumping of reagents and samples. Therefore, it is important to evaluate
285 the stability and the potential chemical modification of the surfaces of the closed channels of the
286 3D printed platforms by the chemicals that will be used in the ensuing CL reactions (see SI for
287 details and Table S1). Our experimental finding however revealed that the surface groups of the
288 printed resin were not changed for any of the tested solutions in this work as appreciated by FT-
289 IR attenuated total reflectance (ATR) spectroscopy (see Fig. S3). Therefore, the immobilization
290 of the CL reagents onto the post-processed 3D printed cells is proven negligible.

291 The optical properties of 3D printed LFS platforms using Clean resin have been extensively
292 studied elsewhere [28]. Transmittance readouts indicated poor optical transparency at the UV
293 region and the higher end of the visible spectrum, yet with a sharp increase from 420 nm and
294 onwards, thus permitting applicability for light capture at the highest emission wavelength of the
295 luminol-H₂O₂-Co(II) CL system, that is, 430 nm.

296 An important parameter to study in the development of novel flow-cells for flash CL reactions is
297 the actual exposed volume of chemiluminogenic reagents/sample mixture to the detector window.
298 A large volume of liquid in the vicinity of the PTM enables collecting a greater amount of elicited
299 light while minimizing autoabsorption phenomena that might be particularly relevant in
300 biological samples. In our work, the accumulated liquid volume in increasing longitudinal
301 sections (250 μm long each) from the detector window was calculated for each of the printed cells
302 using the geometrical dimensions estimated by SEM (See Fig.3). The cylindrical and pyramidal
303 cross-section shapes are those with the lowest accumulated liquid volume within the first 500 μm
304 (*ca.* 60 and 64 mm^3 , respectively) compared to the semicylindrical, cubic and 5-side prism cross-
305 section features (*ca.* 82, 84 and 82 mm^3 , respectively) corresponding to *ca.* 30% volume
306 difference. The entirely available volume for all cross-section geometries was found at *ca.* 1.5
307 mm vertical distance from PTM expect for the pyramidal shape that is more than 2.25 mm long.
308 It is important to note that the ratio of the volume within the first 250 μm (V_i) to the total cell
309 volume (V_t) (see Fig. 3) is distinguishably lower (*ca.* 10%) for the standard cylindrical cell as
310 compared to the rest of designs (*ca.* 20%), thereby indicating that the new printed configurations
311 might provide superior performance for flash CL reactions. Another interesting observation is
312 that the cross-section geometries that feature *ca.* 80% of the total available volume at shorter
313 distances (1.0 mm) are the cubic and the 5-prism shapes corresponding to *ca.* 168 and 165 mm^3 ,
314 respectively (Fig. 3), and thus they are the most appealing configurations for efficient capture of
315 the elicited light.

316

317 **Characterization of the flow-through CL system**

318 Preliminary studies were undertaken using the 3D printed flow cell with cylindrical cross-section
319 for characterization of the configuration of the hybrid flow system. A T-shaped connector (180°,
320 see Fig. S2A) was modelled in the body of the 3D printed structure to merge the reagent and
321 sample downstream just before entering into the spiral channel. The proposed flow system
322 capitalizes upon discontinuous/pulse sample injection and therefore enables low consumption of
323 sample compared to the conventional FI systems [29-31], which is particularly needed in
324 biological assays (*e.g.* saliva). The use of two stand-alone syringes enables greater versatility in
325 changing volumes and flow-rates with respect to FI manifolds or multisyringe flow injection
326 counterparts [32] in which several syringes operate concomitantly. Chemical parameters (pH, and
327 blank signal minimization) and hydrodynamic parameters (injection volume, flow-rate, and
328 mixture of reagents) were investigated with the automatic flow system aimed at maximizing the
329 CL signal intensity.

330 The pH of the CL reagent is a pivotal parameter for proper Co(II)-catalyzed luminol oxidation by
331 H₂O₂. Based on literature data, a pH ranging from 10-11, namely 10.8 was selected [33,30]. The
332 off-line/on-line preparation of composite reagent (luminol+Co(II)) might significantly influence
333 the intensity of elicited CL light under flowing stream conditions. The use of a previously mixed
334 reagent solution [34,30] was discarded because cobalt hydroxide rather than Co(II) is the
335 thermodynamically stable species at pH 10.8 according to the Pourbaix diagram of the cobalt-
336 water system. Instead, in-situ automatic mixing of the two reagents was performed in-syringe.
337 For this purpose, five segments of 960 μL of luminol were aspirated in tandem with four 50 μL
338 segments of Co(II), and further mixed backward within the 3D printed serpentine reactor toward
339 the flow-cell. Because of the flash characteristics of the CL reaction selected as a model reaction,
340 high flow-rates for mixing sample and reagents are necessary, yet limitation is here given by the
341 stability of the flow-cell under moderately high flow pressures. In line with previous studies
342 [24,30], the flow-rate was set to 1000 μL min⁻¹ for the CL composite reagent (serving as a carrier
343 stream) and 1500 μL min⁻¹ for injection of the standards and samples.

344 Initial tests indicated that the reliability of the flow-through CL method was jeopardized by high
345 and unrepeatably blank signals that are attributed to the generation of reactive oxygen species
346 (ROS) by the photolysis of potential organic components of the distilled/reverse osmosis water
347 feeding the Milli-Q water fabrication system, as reported by other authors [34,35]. Note that ROS
348 traces in the catalyst or chemiluminogenic reagent will merely consume minute amounts of
349 luminol, yet no blank contribution in the CL flow system is expected because the flash CL
350 reaction of contaminant-laden water with luminol will occur in-syringe. The contamination of
351 Milli-Q water with traces of ROS was corroborated by performing increasing volume injections

352 of blank (50, 75, 100 and 125 μL). A linear trend of the peak height *versus* the injection volume
353 was encountered. Removal of trace amounts of H_2O_2 from water by use of a manganese oxide
354 microcolumn [33,36], catalase treatment at appropriate pH [37] or filtration and storage in the
355 dark for at least 2 weeks [30] were reported in the literature. In this work, the latter was selected
356 for the Milli-Q water treatment prior to prepare the blank/standard solutions, the CL reagent, the
357 synthetic seawater and diluted saliva.

358 The sample injection volume was optimized based on the largest possible amount that could be
359 efficiently mixed with the reagent in the way towards the detector. Hence, injection volumes
360 ranging from 25 to 100 μL of sample were evaluated. The appearance of a non-gaussian peak was
361 clearly observed for volumes greater than 50 μL . This was attributed to the fact that the internal
362 surface of the 3D printed flow-cells is quite rough, thereby minimizing radial dispersion and
363 impairing mixing of reagents and sample within the short conduit communicating the confluence
364 point with the inlet of the flow-cell. Therefore, the injection volume was set to 50 μL for the
365 ensuing experiments.

366

367 **Analytical performance and fluid dynamic simulations**

368 The analytical performance of the flowing stream CL methods incorporating 3D printed flow-
369 cells with distinct cross-sectional geometry was evaluated in terms of intermediate precision
370 (intra-day and cell-to-cell reproducibility), limit of detection (LOD) based on the $3S_{\text{blank}}$ criterion,
371 and sensitivity following IUPAC recommendations (see Table 2). Calibration graphs were
372 constructed using eight different H_2O_2 standard concentrations ranging from 50 nM to 1,000 nM.
373 The analytical blank was determined using Milli-Q water, which was analyzed in the same way
374 than the standards and includes any signal contribution associated with the solvent itself (see
375 Experimental). Under the selected experimental conditions, a log-log linear graph typically
376 described in CL assays [34,32,38] of light emission *versus* hydrogen peroxide concentration was
377 found over the range previously mentioned for every individual flow-cell. As can be seen in Table
378 2, linear relationships were found ($R^2 > 0.992$) for all the geometries.

379 The intermediate precision of the CL methods was evaluated using the relative standard deviation
380 (% RSD) of the intra-day ($n = 6$) and cell-to-cell ($n = 3$) data for the overall 3D printed designs at
381 the 100 nM and 500 nM levels. A schematic illustration of the diagram obtained in repeatability
382 studies is shown in Fig. S4. The best intra-day RSD values were found for the cubic (1.7%), 5-
383 side prism (2.6%) and the conventional cylindrical shape (2.1%) geometries. Again, cell-to-cell
384 precision that relies on the geometry-dependent printer reliability and resolution indicates
385 superior performance for the cubic (5.7%), 5-side prism (5.6%) and the cylindrical (3.4%)
386 counterpart, yet the pyramidal cell RSD increased up to 9.4%. The elevated cell-to-cell RSD of

387 the pyramidal shape is the result of technical issues for reliable point-by-point LFS
388 polymerization of the internal channel without inner support material.

389 The LOD of methods incorporating the various CL cells with 3D-printed T-shaped connectors
390 are similar (see Table 2), within the range of 39-54 nM, except for the 5-side prism cross-sectional
391 flow-cell, which features the lowest LOD value (21 nM). In fact, the LOD of the latter is 57%
392 lower than that of the cylindrical cross-sectional flow-cell. For the sake of comparison, a milled
393 flat spiral cylindrical cell (80 μ L, 1.0 mm i.d., and 14 mm observation window) made of
394 polymethylmethacrylate (PMMA) and sealed with a window of the same material, which was
395 adapted from previous flow systems capitalized on the luminol chemistry [39], was assembled in
396 our manifold. Experimental results obtained under the selected experimental conditions revealed
397 that twice as high CL readouts at the 100 nM H₂O₂ level were obtained for the 3D printed cell
398 with 5-side prism cross-section with twice as low LOD and significantly better repeatability at
399 the 100 nM as compared to the PMMA cell (2.6 % vs 5.4%, respectively).

400 Comparing the CL method sensitivity using the standard cylindrical flow-cell geometry with that
401 of the new four printed designs, statistically higher values were obtained for the semicylindrical,
402 cubic and 5-side prism cross-sections (see Table 2). This behavior can be explained on the basis
403 of the available liquid volume in the vicinity of the detector window. The larger the absolute
404 liquid volume contained in the flow-cell longitudinal section from 0-500 μ m, the greater is the
405 CL method sensitivity. In fact, a lineal relationship (see Fig. S5) was encountered between the
406 estimated liquid volume within the 0-500 μ m against the slope of the calibration curves ($R^2 =$
407 0.980).

408 To understand the impact of the distinct geometries on the analytical performance, the fluid
409 dynamics at the entry of the flow-cells for the concomitant pumping of the composite reagent and
410 sample should be investigated. Computer fluid dynamics (CFD) will shed light into the effect of
411 the cross-sectional geometry on the changes of liquid velocity *vs* position after the mixing of the
412 reagent and sample plugs by plotting flow fields (see Figs 4A-E). According to the CFD results,
413 the pyramidal structure (Fig. 4C) showed the largest percentage of low flow-rate regions (blue
414 and green zones under 2.1 mL min⁻¹, *ca.* 65%) as compared with the nominal flow rate (2.5 mL
415 min⁻¹). On the other hand, the 5-side prism cross-sectional flow-cell (Fig. 4E) showcases the
416 largest velocities with the minimum percentage of green and blue zones (*ca.* 15%), followed by
417 the cubic, semicylindrical and cylindrical flow-cells (*ca.* 25% of low flow-rate regions). This is
418 in good agreement with the sensitivity and LOD data reported in Table 2, because the greater the
419 flow-rate at the inlet of the spirally-shaped cell and within the detection zone for CL flash
420 reactions the larger is the amount of elicited light efficiently captured by the PTM. Therefore, the
421 5-side prism cross-section geometry was selected for further studies on account of featuring the
422 lowest LOD values and improved sensitivity against those of the cylindrical geometry.

423 The effect of the confluence type upon mixing of reagents and sample towards the flow-cell was
424 further explored. In this sense, 3D-printed Y and Y'-type confluence arrangements (right angle
425 between inlets and 135° or 90° between inlets and outlet, see Fig. S2B and S6B, and Fig. S2C and
426 S6C, respectively) were compared against the previously used T-shape connector (Fig. S2A and
427 S6A). The intra-day repeatability (%RSD) (n = 6) and the cell-to-cell precision (n = 3) of the CL
428 methods were quite similar for the T and Y shapes, which feature satisfactory RSD values (2.6
429 and 5.6% for the T-confluence, and 1.0 and 4.8% for the Y-confluence, respectively, see Table
430 2). On the other hand, the intra-day and cell-to-cell RSDs of the Y'-type cell, because of technical
431 difficulties for repeatable printing of the conduit intersection, increased up to 8.3% and 12.9%,
432 respectively. Regarding LODs of the different flow confluences (T, Y and Y'), twice as much
433 better LOD was achieved with the Y-confluence (*viz.*, 12 nM). The CFD simulation demonstrates
434 that the Y-type connector eliminates the dispersion of the reagent flow into the sample conduit
435 (Fig. S6B) as opposed to the T arrangement (Fig. S6A), and thus, the injection of prior 10 µL-
436 sample into the reagent stream as explained in the analytical method (see Experimental) is now
437 proven unnecessary. In addition, the Y'-type confluence gives rise to partial deviation from the
438 conventional laminar flow (Fig. S6C) expected in flow injection, which results in poorer precision
439 values. Overall, the Y-type confluence demonstrated better analytical performance because it
440 enables appropriate mixing of reagents by confluencing the streams in a radial rather than axial
441 manner [40]. The analytical performance of the CL flow method incorporating the LFS-printed
442 cell with 5-side prism cross-section and Y-confluence was compared against that of two novel
443 designs recently reported in the literature for the luminol-H₂O₂-Co(II) system, namely a Polyjet-
444 printed radial flow-through cell [24] and a hollow bulb-shaped cell [41]. The LOD of our method
445 is one decade better than those of the previous designs the applicability of which to real samples
446 were only demonstrated for food commodities and pharmaceutical formulations at the µM level.

447 Analytical applicability of the 3D printed 5-side prism flow-cell with the Y-type confluence was
448 assessed for samples with a broad range of hydrogen peroxide concentrations and high matrix,
449 such as seawater and human saliva. Samples were spiked at realistic concentrations, that is,
450 nmol/L concentration levels for seawater [33], and µmol/L levels in saliva according to the
451 findings by Chitra *et al.* [42] and the total ROS content in saliva reported by Roy *et al.* [43].
452 Matrix interfering effects onto the CL response were evaluated by comparing the external
453 calibration in Milli-Q water with those obtained by matrix-match using undiluted synthetic
454 seawater, and saliva at 1:400 and 1:1000 dilution factors. The sensitivity ratios of the external to
455 seawater calibration and external to 1:1000 diluted saliva were 0.99 and 0.94, respectively, thus
456 suggesting the lack of multiplicative matrix interferences. Hence, external calibration was
457 selected for the recovery studies in saline waters and saliva. However, should the 1:400 or lower
458 saliva dilution be needed the method of the standard addition had better use instead. The relative

1
2
3
4
5
6
7
8
9
10
11
12
13
14
15
16
17
18
19
20
21
22
23
24
25
26
27
28
29
30
31
32
33
34
35
36
37
38
39
40
41
42
43
44
45
46
47
48
49
50
51
52
53
54
55
56
57
58
59
60
61
62
63
64
65

459 recoveries in seawater at the 116 nM and 232 nM levels, and saliva (diluted 1:1000) at the 0.23
460 and 0.46 mM levels were 96.7% and 82.7%, respectively, for seawater, and 101.0% and 102.9%,
461 respectively, for saliva, with deviation in all cases $\leq 17\%$ thus demonstrated the trueness and the
462 reliability of the automatic CL method incorporating the 3D printed pentagonal cell.

463

464 **CONCLUSIONS**

465 The unique opportunities of LFS for expedient one-step prototyping of microscale platforms that
466 are not available by any other alternative subtractive fabrication approach (e.g. high precision
467 milling) or more sophisticated printing technologies are in this work fully demonstrated with the
468 printing of up to twenty CL flow cells with unrivalled cross-sectional geometry. By designing
469 novel components of flow systems, *namely*, flow-through cells, tailored reactors and mixing
470 zones with convoluted architectures, the applicability of the fourth generation of flow analysis,
471 so-called 3D- μ FIA [44] can be further expanded. Intricate geometries for the spirally-shaped CL
472 cells (e.g., 5-side prism cross-section), the reaction module, and the confluence zone just in front
473 of the detection window have been herein proven superb for improving the analytical performance
474 of flash CL methods (e.g., those based in luminol- H_2O_2 -catalyst chemistry) against the
475 conventional coiled tubing or methacrylate-milled spiral cells with cylindrical cross-section by
476 (i) enhancing forward-flow mixing of sample and reactants, and liquid velocities at the flow cell
477 entry as demonstrated by dynamic fluid simulations and (ii) improving the capture of elicited light
478 by maximizing the solvent volume in the vicinity of the PMT window. Scaffolds as obtained by
479 3D printing also aided at reliably positioning the flow-cell onto the detection window. The
480 incorporation of the 3D printed modules in a hybrid flow system that enabled in-situ preparation
481 of the composite CL reagent fostered unsupervised detection of hydrogen peroxide at
482 concentration levels down to 12 nM as demanded in seawater analysis. Further work is underway
483 to leverage the simplicity of 3D printing for fast prototyping of novel architectures to design CL
484 cells adaptable to other chemistries, to glow-type CL reactions and to the detection of other
485 reactive oxygen species (e.g. superoxide anion) in challenging matrices, such as those involving
486 cell cultures.

487 **Acknowledgements**

488 Manuel Miró and Enrique J. Carrasco-Correa acknowledge financial support from the Spanish
489 State Research Agency (Agencia Estatal de Investigación, AEI/10.13039/501100011033), the
490 Spanish Ministry of Science and Innovation (Ministerio de Ciencia e Innovación, MCIN) and
491 the European Union (NextGenerationEU/PRTR) through projects PID2020-117686RB-C33
492 (AEI/MCIN) and TED2021-131303B-I00 (MCIN/AEI/NextGenerationEU/PRTR). Lluçia

493 Garcia-Moll is grateful to MCIN for funding an FPI-fellowship (PRE2021-100217). Enrique J.
494 Carrasco-Correa also acknowledges the funding of the project PID2021-125459OB-I00 by the
495 AEI (10.13039/501100011033) and the MCIN and the project CIGE/2021/117 funded by
496 Generalitat Valenciana. Alexandra Sixto acknowledges the financial support from the UIB as a
497 Visiting Professor, and to the Agencia Nacional de Investigación e Innovación (ANII,
498 Uruguay).

499

500

501 **Figure captions**

502

503 **Figure 1-**Schematic illustration of the flow manifold assembled for investigation of the analytical
504 features of 3D-printed flow-cells with distinct cross-sectional geometries for the
505 chemiluminescence detection of hydrogen peroxide: A) Coiled flow-cell design, B) Serpentine
506 mixing coil and C) Flow manifold

507

508

509 **Figure 2-**SEM micrographs of the cylindrical (a), semicylindrical (b), pyramid shape (c), cubic
510 (d) and 5-side prism (e) geometries of the spirally-shaped channels of the 3D printed flow-cells.

511

512

513 **Figure 3-** Relative accumulated volume (%) of the different flow-cells at varied longitudinal
514 sections from the detector window as calculated from the experimental geometrical features
515 obtained by SEM (Fig. 2).

516

517

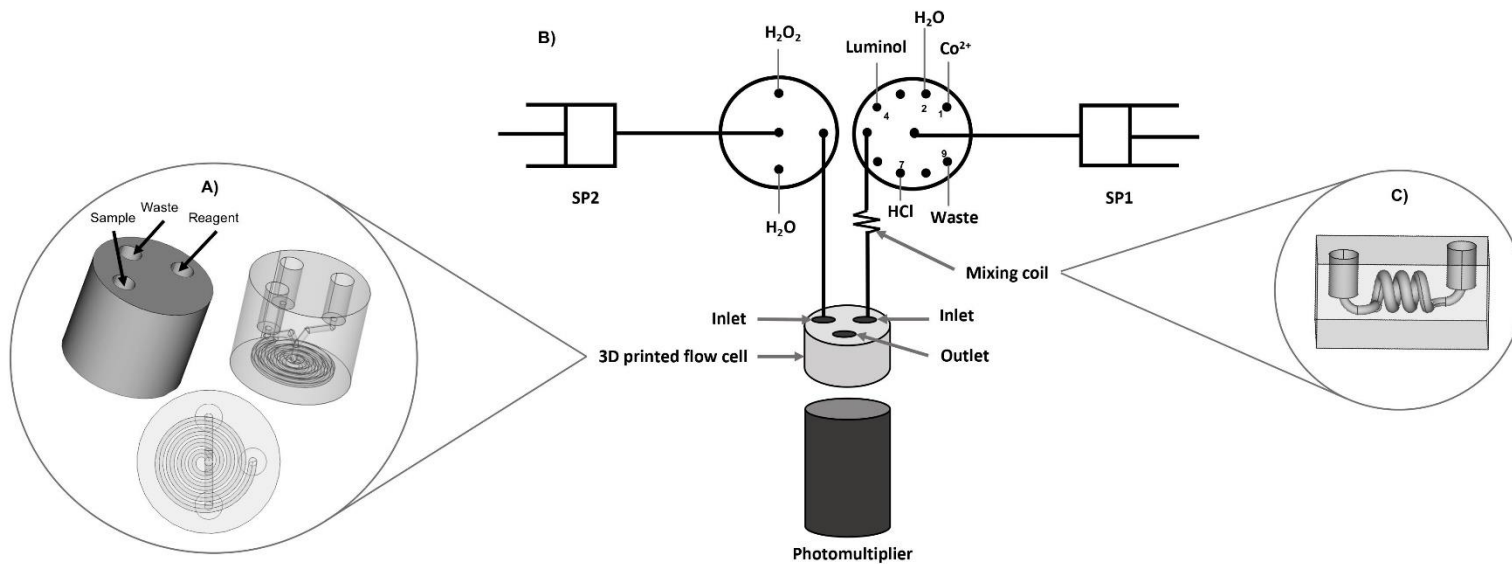
518 **Figure 4-**Computer flow dynamics of the fluid motion (reagent + sample) at the inlet of the flow-
519 cells with varied cross-sectional flow-cell geometries: cylindrical (A), semicylindrical (B),
520 pyramid (C), cubic (D) and 5-side prism (E).

521

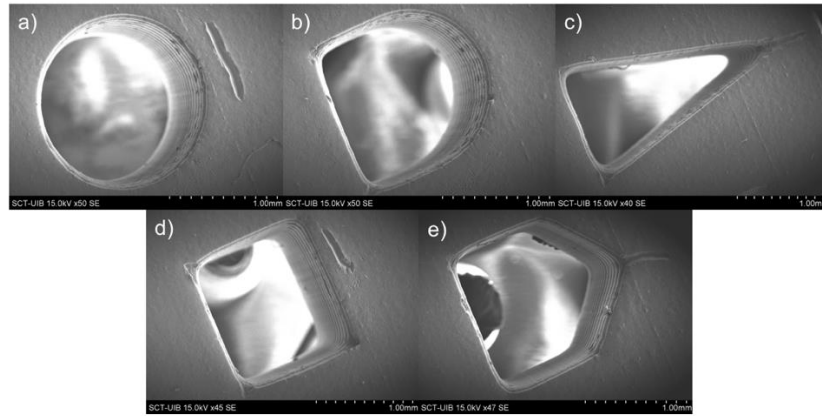
522

16
17
18
19
20
21
22
23
24
25
26
27
28
29
30
31
32
33
34
35
36
37
38
39
40
41
42
43
44
45
46
47
48
49
50
51
52
53
54
55
56
57
58
59
60
61
62
63
64
65

Figure 1



1
2
3 **Figure 2**
4
5



16
17
18
19
20
21
22
23
24
25
26
27
28
29
30
31
32
33
34
35
36
37
38
39
40
41
42
43
44
45
46
47
48
49
50
51
52
53
54
55
56
57
58
59
60
61
62
63
64
65

Figure 3

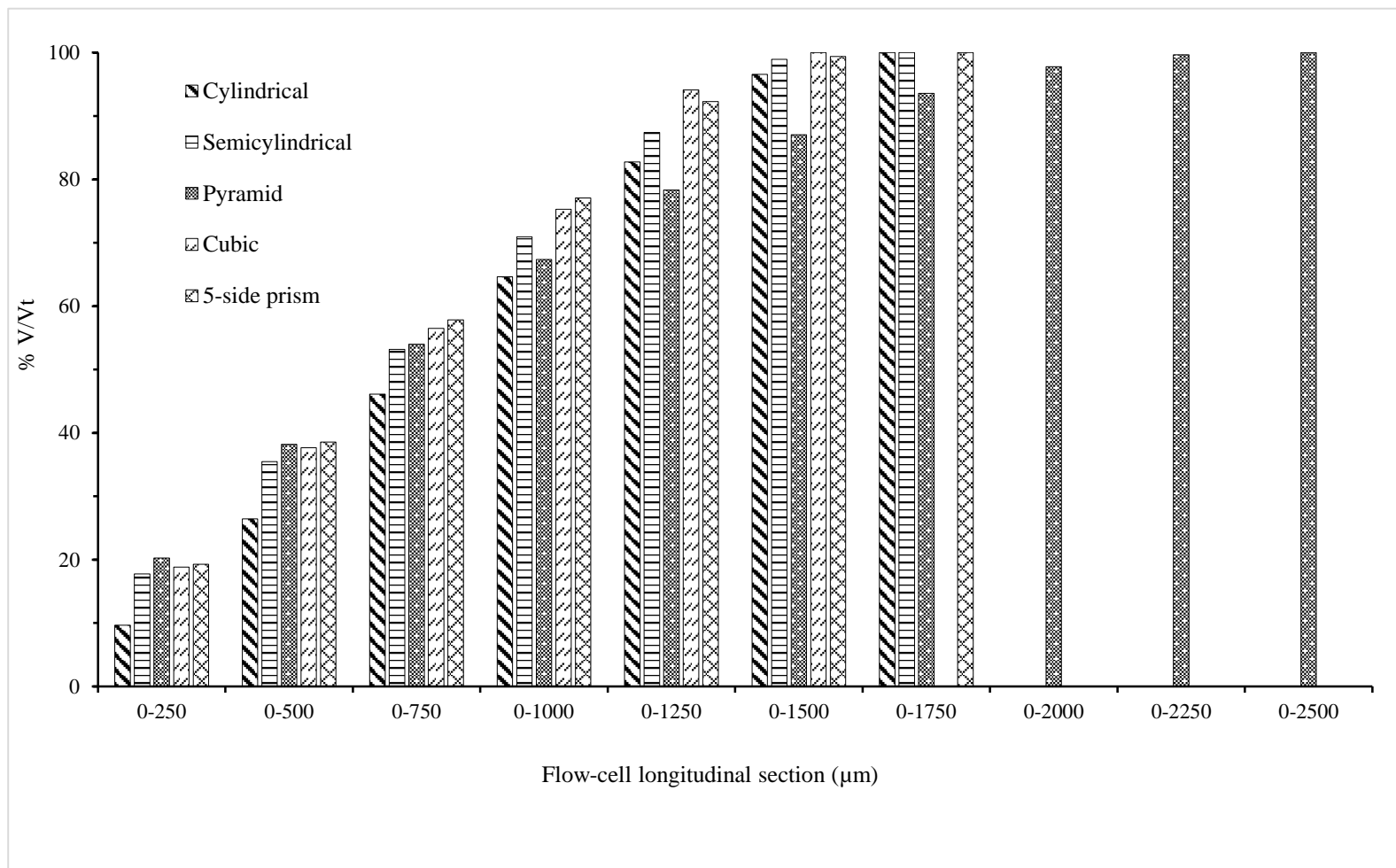


Figure 4

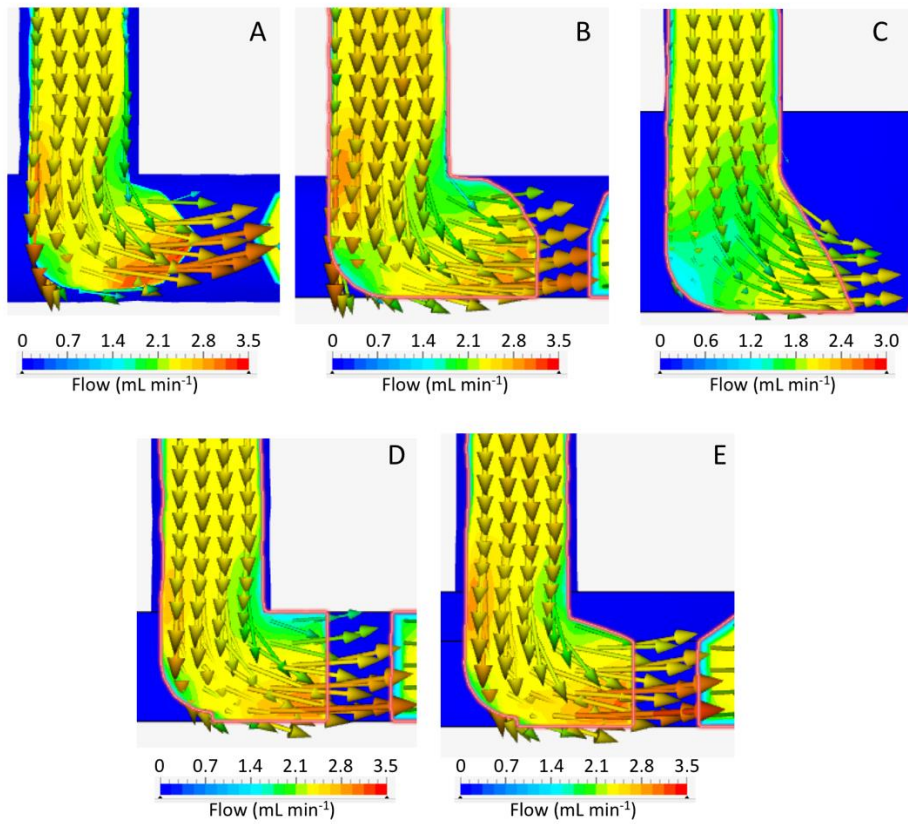


Table 1. Estimation of the volume of the 3D printed flow-cells using the SEM micrographs as compared to nominal values.

| Flow-cell geometry | Theoretical Volume (mm³) | Estimated Volume (mm³)/RSD (%) | Volume difference (%) |
|---------------------------|--|--|----------------------------------|
| Cylindrical | 221 | 227 ± 4 / 1.8 | 2.8 |
| Semicylindrical | 221 | 230 ± 2 / 0.9 | 4.3 |
| Pyramid shape | 221 | 166 ± 12 / 7.2 | -25.0 |
| Cubic | 221 | 223 ± 8 / 3.6 | 0.7 |
| 5-side prism | 221 | 213 ± 11 / 5.2 | -3.5 |

15
16
17
18
19
20
21
22
23
24
25
26
27
28
29
30
31
32
33
34
35
36
37
38
39
40
41
42
43
44
45
46
47
48
49
50
51
52
53
54
55
56
57
58
59
60
61
62
63
64
65

Table 2. Analytical figures of merit of flow-through CL methods incorporating 3D printed cells for determination of hydrogen peroxide as a model analyte

| Flow-cell | Precision at 100 nM level (%) | | LOD (nM) | Sensitivity /t _{exp} | R ² |
|-----------------------------------|-------------------------------|--------------|----------|---------------------------------|----------------|
| | Intra-day | Cell-to-cell | | | |
| Cylindrical (T-shaped) | 2.1 | 3.4 | 49 | 1.01 ± 0.02 /- | 0.997 |
| Semicylindrical (T-shaped) | 4.1 | 6.2 | 54 | 1.37 ± 0.06 / 2.97 ¹ | 0.993 |
| Pyramid (T-shaped) | 7.8 | 9.4 | 49 | 1.13 ± 0.04 / 1.26 ¹ | 0.997 |
| Cubic (T-shaped) | 1.7 | 5.7 | 39 | 1.38 ± 0.04 / 3.69 ¹ | 0.998 |
| 5-side prism (T-shaped) | 2.6 | 5.6 | 21 | 1.39 ± 0.03 / 4.08 ¹ | 0.999 |
| 5-side prism (Y-shaped) | 1.0 | 4.8 | 12 | 1.44 ± 0.06 / 0.81 ² | 0.995 |
| 5-side prism (Y'-shaped) | 3.9 | 12.9 | 48 | 1.19 ± 0.06 / 2.01 ² | 0.995 |

¹ Comparing the sensitivity versus that of the cylindrical (T-shaped) flow-cell at $\alpha=0,05$ for 8 degrees of freedom [45]. $t_{crit}=2.31$

² Comparing the sensitivity versus that of the 5-side prism (T-shaped) flow-cell at $\alpha=0,05$ for 6 degrees of freedom [45]. $t_{crit}=2.45$

REFERENCES

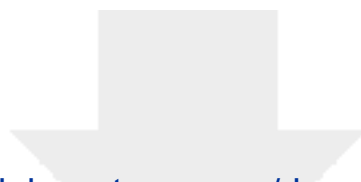
- [1] P.N. Nesterenko, 3D printing in analytical chemistry: Current state and future. *Pure Appl. Chem.* 92 (2020) 1341-1355. DOI: [10.1515/pac-2020-0206](https://doi.org/10.1515/pac-2020-0206).
- [2] A. Ambrosi, A. Bonanni, How 3D printing can boost advances in analytical and bioanalytical chemistry. *Microchim. Acta* 188 (2021) 265 DOI: [10.1007/s00604-021-04901-2](https://doi.org/10.1007/s00604-021-04901-2).
- [3] V. Gupta, P.N. Nesterenko, B. Paull, 3D Printing in Chemical Sciences. The Royal Society of Chemistry, Cambridge, UK, 2019.
- [4] J.S. Stefano, C. Kalinke, R.G. da Rocha, D.P. Rocha, V.A.O.P. da Silva, J.A. Bonacin, L. Angnes, E.M. Richter, B.C. Janegitz, R.A.A. Muñoz, Electrochemical (Bio)Sensors enabled by fused deposition modeling-based 3d printing: a guide to selecting designs, printing parameters, and post-treatment protocols. *Anal. Chem.* 94 (2022) 6417-6429. DOI: [10.1021/acs.analchem.1c05523](https://doi.org/10.1021/acs.analchem.1c05523).
- [5] J. Muñoz, M. Pumera, 3D-printed biosensors for electrochemical and optical applications. *TrAC - Trends Anal. Chem.* 128 (2020) 115933 DOI: [10.1016/j.trac.2020.115933](https://doi.org/10.1016/j.trac.2020.115933).
- [6] F. Li, N.P. Macdonald, R.M. Guijt, M.C. Breadmore, Increasing the functionalities of 3D printed microchemical devices by single material, multimaterial, and print-pause-print 3D printing. *Lab Chip.* 19 (2019) 35-49 DOI: [10.1039/c8lc00826d](https://doi.org/10.1039/c8lc00826d).
- [7] D.J. Cocovi-Solberg, P.J. Worsfold, M. Miró, Opportunities for 3D printed millifluidic platforms incorporating on-line sample handling and separation. *TrAC - Trends Anal. Chem.* 108 (2018) 13-22 DOI: [10.1016/j.trac.2018.08.007](https://doi.org/10.1016/j.trac.2018.08.007).
- [8] H.K. Balakrishnan, E.H. Doeven, A. Merenda, L.F. Dumée, R.M. Guijt, 3D printing for the integration of porous materials into miniaturised fluidic devices: A review. *Anal. Chim. Acta* 1185 (2021) 338796. DOI: [10.1016/j.aca.2021.338796](https://doi.org/10.1016/j.aca.2021.338796).
- [9] F. Li, M.R. Ceballos, S.K. Balavandy, J. Fan, M.M. Khataei, Y. Yamini, F. Maya, 3D Printing in analytical sample preparation. *J. Sep. Sci.* 43(2020) 1854-1866 DOI: [10.1002/jssc.202000035](https://doi.org/10.1002/jssc.202000035).
- [10] C.K. Su, Review of 3D-Printed functionalized devices for chemical and biochemical analysis. *Anal. Chim. Acta* 1158 (2021) 338348. DOI: [10.1016/j.aca.2021.338348](https://doi.org/10.1016/j.aca.2021.338348).
- [11] M. Belka, T. Bączek, Additive manufacturing and related technologies – The source of chemically active materials in separation science. *TrAC - Trends Anal. Chem.* 142 (2021) 116322. DOI: [10.1016/j.trac.2021.116322](https://doi.org/10.1016/j.trac.2021.116322).
- [12] U. Kalsoom, P.N. Nesterenko, B. Paull, Current and future impact of 3D printing on the separation sciences. *TrAC - Trends Anal. Chem.* 105 (2018) 492-502. DOI: [10.1016/j.trac.2018.06.006](https://doi.org/10.1016/j.trac.2018.06.006).

- 1
2
3
4
5
6
7
8
9
10
11
12
13
14
15
16
17
18
19
20
21
22
23
24
25
26
27
28
29
30
31
32
33
34
35
36
37
38
39
40
41
42
43
44
45
46
47
48
49
50
51
52
53
54
55
56
57
58
59
60
61
62
63
64
65
- [13] E.J. Carrasco-Correa, E.F. Simó-Alfonso, J.M. Herrero-Martínez, M. Miró, The emerging role of 3D printing in the fabrication of detection systems. *TrAC - Trends Anal. Chem.* 136 (2021) 116177. DOI: [10.1016/j.trac.2020.116177](https://doi.org/10.1016/j.trac.2020.116177).
- [14] G.I.J. Salentijn, P.E. Oomen, M. Grajewski, E. Verpoorte, Fused deposition modeling 3D printing for (bio)analytical device fabrication: procedures, materials, and applications. *Anal. Chem.* 89 (2017) 7053-7061. DOI: [10.1021/acs.analchem.7b00828](https://doi.org/10.1021/acs.analchem.7b00828).
- [15] R.M. Cardoso, C. Kalinke, R.G. Rocha, P.L. Dos Santos, D.P. Rocha, P.R. Oliveira, B.C. Janegitz, J.A. Bonacin, E.M. Richter, R.A.A. Munoz, Additive-manufactured (3D-printed) electrochemical sensors: A critical review. *Anal. Chim. Acta* 1118 (2020) 73-91 DOI: [10.1016/j.aca.2020.03.028](https://doi.org/10.1016/j.aca.2020.03.028).
- [16] Y. Liang, Q. Liu, S. Liu, X. Li, Y. Li, M. Zhang, One-step 3D printed flow cells using single transparent material for flow injection spectrophotometry. *Talanta* 201 (2019) 460-464. DOI: [10.1016/j.talanta.2019.04.009](https://doi.org/10.1016/j.talanta.2019.04.009).
- [17] M. Michalec, R. Koncki, L. Tymecki, Optoelectronic detectors for flow analysis systems manufactured by means of rapid prototyping technology. *Talanta* 198 (2019) 169-178. DOI: [10.1016/j.talanta.2019.01.092](https://doi.org/10.1016/j.talanta.2019.01.092).
- [18] F. Cecil, R.M. Guijt, A.D. Henderson, M. Macka, M.C. Breadmore, One step multi-material 3D printing for the fabrication of a photometric detector flow cell. *Anal. Chim. Acta* 1097 (2020) 127-134. DOI: [10.1016/j.aca.2019.10.075](https://doi.org/10.1016/j.aca.2019.10.075).
- [19] J. Huang, Q. Qin, J. Wang, A review of stereolithography: Processes and systems. *Processes* 8 (2020) 1138. DOI: [10.3390/PR8091138](https://doi.org/10.3390/PR8091138).
- [20] V. Cannizzaro, A.R. Bowie, A. Sax, E.P. Achterberg, P.J. Worsfold, Determination of cobalt and iron in estuarine and coastal waters using flow injection with chemiluminescence detection. *Analyst* 125 (2000) 51-57. DOI: [10.1039/a907651d](https://doi.org/10.1039/a907651d).
- [21] R.U. Shelley, B. Zachhuber, P.N. Sedwick, P.J. Worsfold, M.C. Lohan, Determination of total dissolved cobalt in UV-irradiated seawater using flow injection with chemiluminescence detection. *Limnol. Oceanogr. Methods* 8 (2010) 352-362. DOI: [10.4319/lom.2010.8.352](https://doi.org/10.4319/lom.2010.8.352).
- [22] J.M. Terry, E.M. Zammit, T. Slezak, N.W. Barnett, D.C. Olson, D.K. Wolcott, D.L. Edwards, P.S. Francis, Solution mixing and the emission of light in flow-cells for chemiluminescence detection. *Analyst* 136 (2011) 913-919 DOI: [10.1039/c0an00591f](https://doi.org/10.1039/c0an00591f).
- [23] K.B. Spilstead, J.J. Learey, E.H. Doeven, G.J. Barbante, S. Mohr, N.W. Barnett, J.M. Terry, R.M. Hall, P.S. Francis, 3D-printed and CNC milled flow-cells for chemiluminescence detection. *Talanta* 126 (2014) 110-115 DOI: [10.1016/j.talanta.2014.03.047](https://doi.org/10.1016/j.talanta.2014.03.047).
- [24] V. Gupta, P. Mahbub, P.N. Nesterenko, B. Paull, A new 3D printed radial flow-cell for chemiluminescence detection: Application in ion chromatographic determination of

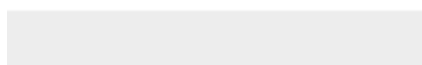
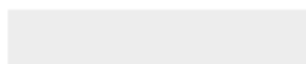
- hydrogen peroxide in urine and coffee extracts. *Anal. Chim. Acta* 1005 (2018) 81-92. DOI: [10.1016/j.aca.2017.12.039](https://doi.org/10.1016/j.aca.2017.12.039).
- [25] R. G. Wetzel, G. E. Likens, *Limnological Analyses* (3rd Edn), Springer New York, 2000. DOI: 10.1007/978-1-4757-3250-4
- [26] D.J. Cocovi-Solberg, M. Miró, *CocoSoft: Educational software for automation in the analytical chemistry laboratory*. *Anal. Bioanal. Chem.* 407 (2015) 6227-6233. DOI: [10.1007/s00216-015-8834-8](https://doi.org/10.1007/s00216-015-8834-8).
- [27] F.A.S. Vaz, L.N.O. Neves, R. Marques, R.T. Sato, M.A.L. Oliveira, *Chromophoreasy, an excel-based program for detection and integration of peaks from chromatographic and electromigration techniques*. *J. Braz. Chem. Soc.* 27 (2016) 1899-1911. DOI: [10.5935/0103-5053.20160076](https://doi.org/10.5935/0103-5053.20160076).
- [28] D.J. Cocovi-Solberg, M. Rosende, M. Michalec, M. Miró, *3D Printing: The second dawn of Lab-on-Valve fluidic platforms for automatic (bio)chemical assays*. *Anal. Chem.* 91 (2019) 1140-1149. DOI: [10.1021/acs.analchem.8b04900](https://doi.org/10.1021/acs.analchem.8b04900).
- [29] P.J. Worsfold, R. Clough, M.C. Lohan, P. Monbet, P.S. Ellis, C.R. Quétel, G.H. Floor, I.D. McKelvie, *Flow injection analysis as a tool for enhancing oceanographic nutrient measurements-A review*. *Anal. Chim. Acta* 803 (2013) 15-40. DOI: [10.1016/j.aca.2013.06.015](https://doi.org/10.1016/j.aca.2013.06.015).
- [30] A. Milne, M.S. Davey, P.J. Worsfold, E.P. Achterberg, A.R. Taylor, *Real-time detection of reactive oxygen species generation by marine phytoplankton using flow injection-chemiluminescence*. *Limnol. Oceanogr. Methods* 7 (2009) 706-715. DOI: [10.4319/lom.2009.7.706](https://doi.org/10.4319/lom.2009.7.706).
- [31] J.A. Murillo-Pulgarín, L.F. García-Bermejo, A. Carrasquero-Durán, *A fast and simple FIA-chemiluminescence method for the evaluation of Roselle flowers as scavenger of the free radicals generated by UV irradiated antibiotics*. *J. Pharm. Biomed. Anal.* 164 (2019) 630-635. DOI: [10.1016/j.jpba.2018.11.004](https://doi.org/10.1016/j.jpba.2018.11.004).
- [32] M. Manera, M. Miró, J.M. Estela, V. Cerdà, *A multisyringe flow injection system with immobilized glucose oxidase based on homogeneous chemiluminescence detection*. *Anal. Chim. Acta* 508 (2004) 23-30. DOI: [10.1016/j.aca.2003.11.050](https://doi.org/10.1016/j.aca.2003.11.050).
- [33] D. Price, P.J. Worsfold, R. Fauzi, C. Mantoura, *Determination of hydrogen peroxide in sea water by flow-injection analysis with chemiluminescence detection*. *Anal. Chim. Acta* 298 (1994) 121-128. DOI: [10.1016/0003-2670\(94\)90050-7](https://doi.org/10.1016/0003-2670(94)90050-7).
- [34] S. Uchida, Y. Satoh, N. Yamashiro, T. Satoh, *Determination of hydrogen peroxide in water by chemiluminescence detection, (II) theoretical analysis of luminol chemiluminescence processes*. *J. Nucl. Sci. Technol.* 41 (2004) 898-906. DOI: [10.1080/18811248.2004.9715562](https://doi.org/10.1080/18811248.2004.9715562).
- [35] S. Garg, A.L. Rose, T.D. Waite, *Production of reactive oxygen species on photolysis of*

dilute aqueous quinone solutions. *Photochem. Photobiol.* 83 (2007) 904-913 DOI: [10.1111/j.1751-1097.2007.00075.x](https://doi.org/10.1111/j.1751-1097.2007.00075.x).

- [36] W.J. Cooper, J.K. Moegling, R.J. Kieber, J.J.A. Kiddle, A chemiluminescence method for the analysis of H₂O₂ in natural waters. *Mar. Chem.* 70 (2000) 191-200. DOI: [10.1016/S0304-4203\(00\)00025-6](https://doi.org/10.1016/S0304-4203(00)00025-6).
- [37] D.W. King, W.J. Cooper, S.A. Rusak, B.M. Peake, J.J. Kiddle, D.W. O'Sullivan, M.L. Melamed, C.R. Morgan, S.M. Theberge, Flow injection analysis of H₂O₂ in natural waters using acridinium ester chemiluminescence: Method development and optimization using a kinetic model. *Anal. Chem.* 79 (2007) 4169-4176. DOI: [10.1021/ac062228w](https://doi.org/10.1021/ac062228w).
- [38] A. Townshend, R.A. Wheatley, Oxidative chemiluminescence assay of 2,4-dinitrophenylhydrazine. *Analyst* 123 (1998) 1041-1046. DOI: [10.1039/a708350e](https://doi.org/10.1039/a708350e).
- [39] M. Manera, M. Miró, M.F. Ribeiro, J.M. Estela, V. Cerdà, J.J. Santos, J.LF.C. Lima, Rapid chemiluminometric determination of gabapentin in pharmaceutical formulations exploiting pulsed-flow analysis. *Luminescence* 24 (2009) 10-14 DOI: [10.1002/bio.1055](https://doi.org/10.1002/bio.1055).
- [40] J. Ruzicka, E.H. Hansen, *Flow Injection Analysis*, 2nd edn., John Wiley, New York, 1988, pp. 152-154
- [41] E.G. Brandão, S.R.W. Perdigão, B.F. Reis, A new flow cell design for chemiluminescence detection using an improved signal transduction network. Determination of hydrogen peroxide in pharmaceuticals. *Microchem. J.* 171 (2021) 106789. DOI: [10.1016/j.microc.2021.106789](https://doi.org/10.1016/j.microc.2021.106789).
- [42] S. Chitra, M. Balasubramaniam, J. Hazra, Effect of α -tocopherol on salivary reactive oxygen species and trace elements in oral submucous fibrosis. *Ann. Clin. Biochem.* 49 (2012) 262-265. DOI: [10.1258/acb.2011.011050](https://doi.org/10.1258/acb.2011.011050).
- [43] J. Roy, N. Manjunath, K. Bhat, A. George, F. Nishana, L. Mathew, Estimation of salivary glycoconjugates and salivary ros levels in chronic periodontitis: a clinico-biochemical study. *Int. J. Res. Med. Sci.* 5 (2017) 3578-3583. DOI: [10.18203/2320-6012.ijrms20173566](https://doi.org/10.18203/2320-6012.ijrms20173566).
- [44] H. Wang, D.J. Cocovi-Solberg, B. Hu, M. Miró, 3D-Printed Microflow Injection Analysis Platform for Online Magnetic Nanoparticle Sorptive Extraction of Antimicrobials in Biological Specimens as a Front End to Liquid Chromatographic Assays. *Anal. Chem.* 89 (2017) 12541-12549. DOI: [10.1021/acs.analchem.7b03767](https://doi.org/10.1021/acs.analchem.7b03767).
- [45] D.L. Massart, B.G.M. Vandeginste, L.M.C. Buydens, S. De Jong, P.J. Lewi, J. Smeyers-Verbeke, *Handbook of Chemometrics and Qualimetrics: Part A, Volume 20A*. Elsevier, The Netherlands, 1998.



Click here to access/download
Supplementary Material
Supporting Info-FINAL-Talanta.docx



DECLARATION OF INTEREST STATEMENT

The authors declare that there are no known conflicts of interest to disclose

CRedit author statement

Llucia García-Moll: Investigation, Formal Analysis, Writing-original draft, Visualization

Alexandra Sixto: Methodology, Investigation, Formal Analysis, Validation, Writing-original draft

Enrique J. Carrasco-Correa: Conceptualization, Methodology, Formal Analysis, Writing-review&editing, Supervision

Manuel Miró: Conceptualization, Methodology, Writing-review&editing, Supervision, Project administration, funding acquisition

Checklist

1. Cover letter
2. Novelty statement
3. Highlights
4. Graphical abstract
5. List of reviewers
6. Manuscript
7. Supplementary Material
8. Declaration statement
9. Credit Author Statement